arXiv:2603.02767v2 [cs.CV] 4 Mar 2026

ITO: Images and Texts as One via Synergizing Multiple Alignment and Training-Time Fusion

HanZpeng Liu [1 2] **Yaqian Li** [2] **Zidan Wang** [1] **Shuoxi Zhang** [3] **Zonglin Zhao** [1] **Zihao Bo** [2] **Rinyoichi Takezoe** [2] **Kaiwen Long** [2] **Kun He** [1]

Abstract

Image–text contrastive pretraining has become a dominant paradigm for visual representation learning, yet existing methods often yield representations that remain partially organized by modality. We propose **ITO**, a framework addressing this limitation through two synergistic mechanisms. *Multimodal multiple alignment* enriches supervision by mining diverse image–text correspondences, while a lightweight *training-time multimodal fusion* module enforces structured cross-modal interaction. Crucially, the fusion module is discarded at inference, preserving the efficiency of standard dual-encoder architectures. Extensive experiments show that ITO consistently outperforms strong baselines across classification, retrieval, and multimodal benchmarks. Our analysis reveals that while multiple alignment drives discriminative power, training-time fusion acts as a critical **structural regularizer**—eliminating the modality gap and stabilizing training dynamics to prevent the early saturation often observed in aggressive contrastive learning.

1. Introduction

Recent foundation models such as CLIP (Radford et al., 2021; Cherti et al., 2023) have fundamentally reshaped visual representation learning through large-scale image–text contrastive pretraining, demonstrating strong transferability across zero-shot classification, retrieval, and as visual backbones for multimodal large language models (Liu et al., 2024a). A growing body of follow-up work (Mu et al., 2022; Eslami & de Melo, 2025; Xiao et al., 2025) has further strengthened alignment quality and scaling behavior through improved data curation, alternative objectives, and architectural refinements, establishing image–text contrastive learning as a dominant paradigm for large-scale visual pretraining.

Despite this success, alignment alone does not necessarily imply integration. While contrastive objectives encourage instance-level matching between paired images and texts, they do not explicitly constrain how representations are organized globally in the embedding space. In practice, representations learned by dual-encoder contrastive training often remain partially structured by modality, with image and text embeddings forming distinct subspaces even when alignment performance is strong. As we show in Section 4.7, such modality-induced separation persists across different training variants, indicating that standard contrastive objectives may rely on modality-specific shortcuts rather than learning a truly unified semantic space.

This limitation motivates us to ask: *Can we explicitly reduce modality-induced separation in image–text representations while preserving the efficiency and scalability of dual-encoder architectures?* Prior work (Dou et al., 2022; Eslami & de Melo, 2025; Xiao et al., 2025) has explored cross-modal fusion to enhance multimodal interaction. However, existing approaches either introduce fusion modules that remain active at inference (increasing computational cost), or apply fusion through task-specific architectural designs (limiting generalizability). Whether fusion objectives can instead act as a *training signal* to reshape encoder representations themselves—without modifying the inference architecture—remains underexplored.

To address this challenge, we propose **ITO** (Image–Text as One), an image–text contrastive pretraining framework that achieves unified representations through two synergistic mechanisms. First, *Multimodal multiple alignment* densifies the supervision signal by constructing diverse image–text correspondences from augmented views, effectively mining the potential information capacity of the data. Second, ITO introduces a lightweight *training-time multimodal fusion* module that enforces structured cross-modal interaction during optimization. Crucially, this fusion module is used only during training and discarded at inference, allowing ITO

[1]School of Computer Science and Technology, Huazhong University of Science and Technology, Wuhan, China [2]Li Auto Inc. [3]Institute of AI for Industries, Chinese Academy of Sciences. Correspondence to: Kaiwen Long <longkaiwen@lixiang.com>, Kun He <brooklet60@hust.edu.cn>.

Preprint. March 5, 2026.

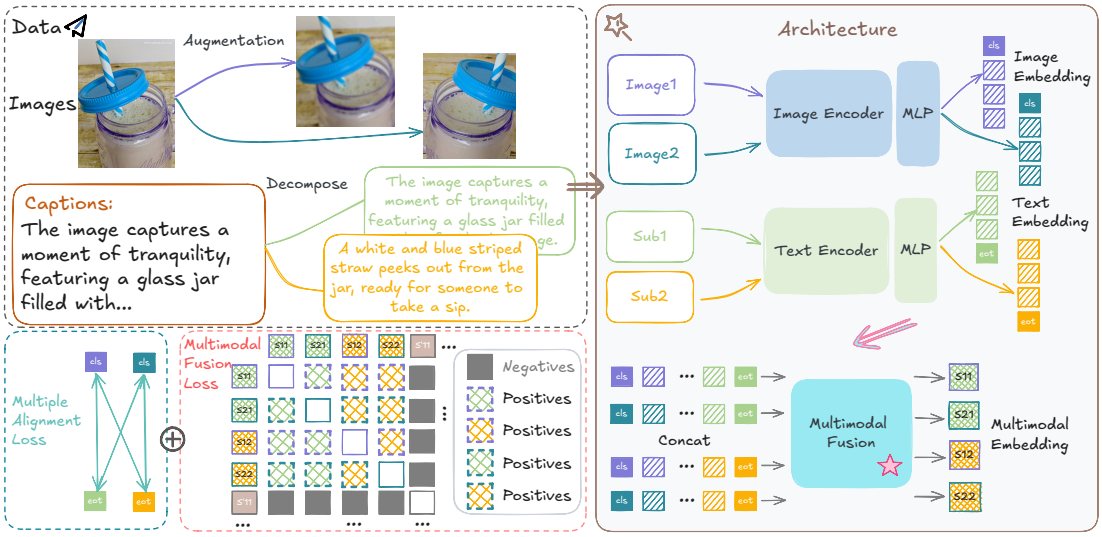

Figure 1. **Overview of the proposed ITO training framework.** Starting from standard image–text contrastive pretraining, ITO restructures supervision through multimodal multiple alignment and introduces a lightweight multimodal fusion module during training. Multiple augmented image–text pairs derived from the same sample are used to enrich instance-level alignment, while training-time fusion enables structured cross-modal interaction and guides the encoders toward more integrated representations. Importantly, the fusion module is used only during training and is discarded at inference time, allowing ITO to retain a standard dual-encoder architecture for efficient deployment.

to retain a standard dual-encoder architecture for efficient deployment. The overall framework of ITO is illustrated in Figure 1.

Our experiments and analysis reveal a critical interplay between these components rather than a simple additive effect. While multiple alignment acts as the primary engine for increasing discriminative power, training-time fusion functions as a necessary **structural regularizer**. We demonstrate that fusion plays a pivotal role in eliminating the modality gap and *stabilizing training dynamics*, effectively preventing the performance saturation and overfitting often observed when scaling up aggressive alignment strategies. Extensive evaluations across zero-shot classification (Barbu et al., 2019; Cimpoi et al., 2014; Veeling et al., 2018; Wang et al., 2019), image–text retrieval, and multimodal benchmarks show that ITO consistently improves representation quality over strong baselines. Beyond empirical performance, our findings highlight that distinguishing *alignment* from *integration* is essential for designing robust objectives in next-generation contrastive pretraining.

2. Related Work

Image–Text Contrastive Learning for Visual Representation Learning. Image–text contrastive learning has emerged as a powerful paradigm for large-scale visual representation learning. CLIP (Radford et al., 2021) demonstrates that aligning images and texts through contrastive objectives enables the learning of highly transferable vision encoders, which generalize effectively across zero-shot classification, linear probing, and image–text retrieval tasks, and are commonly adopted as visual backbones in multimodal large language models (Goyal et al., 2017a). Following this line of work, a number of studies have explored improved data curation, scaling strategies, and alternative contrastive formulations, including SigLIP (Zhai et al., 2023), MetaCLIP (Xu et al., 2024), CyCLIP (Goel et al., 2022), and SuperCLIP (Zhao et al., 2025), further strengthening robustness and scalability of image–text pretraining. Collectively, these methods establish image–text contrastive learning as a dominant weakly supervised paradigm for visual pretraining. Despite their success, most existing approaches primarily focus on improving instance-level alignment between paired images and texts. As a result, they largely treat image–text contrastive learning as a mechanism for matching corresponding samples, without explicitly addressing how representations are globally organized in the shared embedding space. This limitation motivates recent efforts to move beyond alignment and examine deeper structural properties of learned representations.

Strengthening Alignment in Image–Text Contrastive Learning. Recent work has sought to strengthen image–text alignment by enriching supervision signals within contrastive pretraining. On the visual side, SLIP (Mu et al., 2022) improves alignment by enforcing stronger intra-modal visual consistency through image-only augmentations, leading to improved visual representations that benefit image–text contrastive learning. On the textual side, LaCLIP (Fan et al., 2023), VeCLIP (Lai et al., 2024), and DreamLIP (Zheng et al., 2024) expand or refine textual views using large language or vision–language models (Dubey et al., 2024), enhancing the semantic coverage of captions asso-

ciated with each image. While effective, these approaches primarily improve alignment by enhancing the quality or diversity of individual modality views, while preserving the underlying contrastive supervision structure. Image–text relationships remain largely instance-level and one-to-one, without explicitly restructuring cross-modal associations within a batch. In contrast, our Multimodal multiple alignment strategy operates at the level of supervision structure, enabling one-to-many and many-to-many image–text alignment. By exposing the model to diverse cross-modal correspondences during training, it enriches contrastive supervision beyond conventional setups, but alone does not explicitly reshape representation organization, motivating its combination with training-time fusion.

Training-Time Fusion and Cross-Modal Interaction. Beyond alignment-centric approaches, another line of research investigates incorporating cross-modal interaction or fusion mechanisms during pretraining. Models such as FIBER (Dou et al., 2022) and related vision–language architectures introduce cross-attention or joint encoding modules to enable deeper interaction between visual and textual tokens, achieving strong performance on multimodal understanding tasks. AlignCLIP (Eslami & de Melo, 2025) reduces the modality gap by sharing parameters across encoders, while FLAIR (Xiao et al., 2025) employs text-conditioned pooling to induce localized fusion effects. Although these methods demonstrate the effectiveness of fusion for downstream performance, fusion is often tightly coupled with inference-time architectures or task-specific designs. Consequently, it remains unclear whether and how fusion objectives influence the representations learned by standalone encoders, especially when fusion modules are removed at inference time. In particular, existing work provides limited analysis on whether training-time fusion reshapes the organization of the representation space itself, rather than acting as an auxiliary architectural component. In contrast, our work focuses on training-time fusion as a mechanism for shaping representation structure in image–text contrastive pretraining. By decoupling training-time fusion from inference-time deployment, ITO reduces modality-induced separation while preserving the scalability and efficiency of dual-encoder contrastive models.

3. Method

3.1. Preliminaries: CLIP-style Contrastive Pretraining

We build upon the standard image–text contrastive learning framework introduced by CLIP. Given a batch of B image–text pairs $\{(I^n, T^n)\}_{n=1}^{B}$, an image encoder E_I and a text encoder E_T are used to extract visual and textual representations, which are then projected into a shared embedding space via projection heads P_I and P_T:

$$Y^n = P_I(E_I(I^n)), \qquad Z^n = P_T(E_T(T^n)). \tag{1}$$

Image–text alignment is achieved through a symmetric InfoNCE objective. Specifically, the image-to-text and text-to-image losses are defined as

$$\mathcal{L}_{I\to T} = -\sum_{n=1}^{B} \log \frac{\exp\left(\langle Y^n, Z^n\rangle/\tau\right)}{\sum_{m=1}^{B}\exp\left(\langle Y^n, Z^m\rangle/\tau\right)}, \tag{2a}$$

$$\mathcal{L}_{T\to I} = -\sum_{n=1}^{B} \log \frac{\exp\left(\langle Z^n, Y^n\rangle/\tau\right)}{\sum_{m=1}^{B}\exp\left(\langle Z^n, Y^m\rangle/\tau\right)}. \tag{2b}$$

, where $\langle\cdot\rangle$ denotes cosine similarity and τ is a learnable temperature. The overall CLIP loss is given by

$$\mathcal{L}_{CLIP} = \frac{1}{2}(\mathcal{L}_{I\to T} + \mathcal{L}_{T\to I}). \tag{3}$$

This dual-encoder formulation enables efficient and scalable inference, which we preserve throughout this work.

3.2. Multimodal Multiple Alignment

To enrich contrastive supervision beyond one-to-one image–text pairing, we introduce Multimodal multiple alignment, which restructures the supervision signal within a training batch. Instead of treating each image–text pair as a single positive instance, this strategy exposes the model to multiple image–text correspondences derived from the same underlying sample, enabling more flexible instance-level alignment.

Concretely, for each original image–text pair (I_i^n, T_j^n), multiple image–text combinations are constructed through standard image and text perturbations, resulting in a set of augmented pairs $\{(I_i^n, T_j^n)\}$. By default, we use two image views ($i \in \{1, 2\}$) and a single text view ($j = 1$). When two text views are used ($j \in \{1, 2\}$), we refer to the resulting variant as *ITO_sub2*. For clarity, we present the formulation under the *ITO_sub2* setting as an example, with the default ITO configuration being a special case.

For each augmented image–text pair (I_i^n, T_j^n), we compute a bidirectional contrastive loss following the CLIP formulation, including image-to-text and text-to-image directions. Importantly, we retain the standard batch-wise negative sampling strategy: the corresponding augmented pair is treated as the positive sample, while all other samples within the batch serve as negatives. This process is repeated for all valid combinations of image and text views, and the final alignment loss is computed as the average over these losses. Formally, the multiple alignment loss is defined as

$$\mathcal{L}_{\text{Align}} = \frac{1}{4}\sum_{i=1}^{2}\sum_{j=1}^{2}\frac{1}{2}\left[\mathcal{L}_{I_i\to T_j} + \mathcal{L}_{T_j\to I_i}\right], \tag{4}$$

where $\mathcal{L}_{I_i \to T_j}$ and $\mathcal{L}_{T_j \to I_i}$ denote the image-to-text and text-to-image InfoNCE losses, respectively.

By increasing the diversity and number of positive image–text pairings within each batch, Multimodal multiple alignment enriches instance-level supervision and improves alignment robustness without introducing additional inference-time cost. However, this strategy alone does not explicitly constrain how representations are organized in the shared embedding space, motivating the incorporation of training-time multimodal fusion to further reduce modality-induced separation.

3.3. Training-Time Multimodal Fusion

While multiple alignment strengthens correspondence between individual image–text pairs, effective integration of modalities requires structured cross-modal interaction. To this end, we introduce a lightweight training-time multimodal fusion module that guides the encoders toward more integrated representations.

Given an augmented image–text pair (I_i^n, T_j^n), we obtain their corresponding visual tokens Y_i^n and textual tokens Z_j^n. These tokens are concatenated to form a joint multimodal sequence:

$$H_{i,j}^n = \mathrm{Concat}(Y_i^n, Z_j^n), \tag{5}$$

where $\mathrm{Concat}(\cdot,\cdot)$ denotes token-wise concatenation. The joint sequence is then processed by a lightweight fusion module F_M, implemented as a two-layer Transformer with bidirectional attention, producing fused multimodal tokens:

$$S_{i,j}^n = F_M(H_{i,j}^n). \tag{6}$$

We use the token corresponding to the end-of-text position as the fused multimodal representation.

During training, the fusion objective encourages consistency among multimodal representations derived from the same underlying image–text pair, while pushing apart representations from different pairs. Specifically, fused representations obtained from different augmentations of the same image–text pair are treated as positive samples, while fused representations from other samples within the batch serve as negatives. We adopt a contrastive formulation with multiple positives to account for this structure. The loss for a fused representation is defined as:

$$\mathcal{L}_{S_{1,1}^n} = -\log \frac{\exp[\langle S_{1,1}^n \cdot S_{2,1}^n \rangle/\tau] + \sum_{i=1}^{2} \exp[\langle S_{1,1}^n \cdot S_{i,2}^n \rangle/\tau]}{\sum_{m=1}^{B} \sum_{i=1}^{2} \sum_{k=1}^{2} \exp[\langle S_{1,1}^n \cdot S_{i,k}^m \rangle/\tau]}, \tag{7}$$

where the trivial self-pair $(m = n, i = 1, k = 1)$ is excluded. The overall fusion loss is:

$$\mathcal{L}_{\text{Fusion}} = \frac{1}{4B} \sum_{n=1}^{B} \sum_{i=1}^{2} \sum_{j=1}^{2} \mathcal{L}_{S_{i,j}^n}. \tag{8}$$

By propagating gradients through the fusion module back to the individual encoders, L_{Fusion} acts as a soft structural constraint. It forces the encoders to learn features that are not just linearly separable (as in vanilla contrastive learning) but are also compatible for deep fusion. This prevents the distinct encoders from drifting into isolated modality subspaces, effectively acting as a regularizer against modality-specific overfitting.

3.4. Overall Objective and Inference

The final training objective combines the multiple alignment loss and the multimodal fusion loss:

$$\mathcal{L} = \mathcal{L}_{\text{Align}} + \lambda \mathcal{L}_{\text{Fusion}}. \tag{9}$$

Here, λ balances the trade-off between discriminative intensity (from alignment) and geometric regularization (from fusion). At inference time, ITO reduces to a standard dual-encoder model identical to CLIP, without any fusion modules or additional computational overhead. This enables efficient deployment and direct replacement of existing image–text contrastive encoders.

4. Experiments

4.1. Implementation Details

Datasets. We evaluate our method across image–text datasets spanning from millions to billions of samples in order to assess effectiveness, robustness, and scalability. Specifically, we conduct pretraining on Conceptual Captions 3M (CC3M) (Sharma et al., 2018), Conceptual Captions 12M (CC12M) (Changpinyo et al., 2021), and YFCC15M (Torralba & Efros, 2011), which are widely used benchmarks for image–text contrastive pretraining. To study large-scale behavior, we further perform experiments on Laion100M (a 100M subset of Laion400M (Schuhmann et al., 2021)) and the billion-scale DataComp-1B (Gadre et al., 2023) dataset. Due to computational constraints, experiments on Laion100M and DataComp-1B are conducted only for CLIP and our method. Detailed dataset statistics are provided in appendix Table 6.

Data Augmentation. We adopt standard image augmentations following prior work (e.g.,MoCo v3 (Chen et al., 2021) and SLIP (Mu et al., 2022)) to generate two image views per sample. For text, we consider two settings: a default configuration using a single caption, and an optional variant that samples two sub-descriptions from the original text. The latter is denoted as ITO_sub2. Sub-description sampling (ITO_sub2) is applied only to CC3M, CC12M, YFCC15M, and DataComp-1B experiments. These augmentations are used solely to construct multiple views for contrastive supervision and are not central to our method design.

Pretraining Settings. All models are implemented based on OpenCLIP (Cherti et al., 2023). Unless otherwise specified, we use ViT-B/16 as the vision encoder and the standard CLIP text encoder. Images are resized to 224×224, and text sequences are tokenized to a maximum length of 77 tokens. Models are optimized using AdamW with a cosine learning rate schedule and linear warmup. We train models for 30 epochs on CC3M, CC12M, YFCC15M and Laion100M. For DataComp-1B, models are trained for one epoch due to computational cost; an additional 10-epoch ViT-B/16 model is trained to study data scaling effects. Batch size and learning rate are adjusted according to the dataset scale. The fusion loss weight λ is set to 2 by default. All other hyperparameters follow OpenCLIP defaults. All training is conducted on A100 GPUs. To ensure fair comparison, we reproduce these methods using the versions of the datasets we have downloaded.

Evaluation Protocol. We evaluate pretrained models using only the image and text encoders, without any fusion modules, to assess representation quality under a standard dual-encoder setting. Four categories of downstream tasks are considered.

Zero-shot Image Classification. We follow the evaluation protocol of EVA-CLIP (Sun et al., 2023) and report top-1 accuracy on 26 datasets covering generic, fine-grained, and domain-specific classification tasks.

Linear Image Classification. We perform linear probing by training a single linear classifier on frozen visual features, using identical optimization settings for all methods.

Zero-shot Image-Text Retrieval. Bidirectional retrieval is evaluated on COCO (Lin et al., 2014), Flickr30K (Plummer et al., 2015), and DOCCI (Onoe et al., 2024), reporting Recall@1/5/10 for both image-to-text and text-to-image retrieval.

Vision-Language Understanding. To assess transferability to multimodal systems, we follow the official LLaVA-1.5 (Liu et al., 2024a) evaluation protocol on 13 benchmarks, including VQAv2 (Goyal et al., 2017b), MM-Vet (Yu et al., 2024), POPE (Li et al., 2023), and MMStar (Chen et al., 2024b). These experiments evaluate the pretrained visual encoders as backbones rather than introducing new VLM architectures.

All baselines are reproduced and evaluated under the same pipeline for fair comparison and reproducibility.

4.2. Zero-shot Image Classification

We evaluate zero-shot image classification on 26 public benchmarks following the EVA-CLIP (Sun et al., 2023) protocol, covering generic, fine-grained, and domain-specific datasets. Unless otherwise specified, all models use ViT-B/16 and standard CLIP-style prompts. Results are summarized in Table 1, with additional scaling results reported in the appendix Table 8.

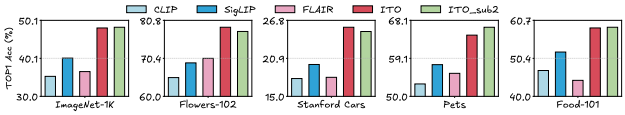

Figure 2. Linear image classification of ITO and its variants pretrained on CC3M.

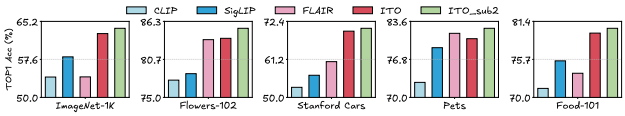

Figure 3. Linear image classification of ITO and its variants pretrained on CC12M.

Across all pretraining datasets, ITO consistently outperforms CLIP (Radford et al., 2021) and strong image–text contrastive baselines, including SLIP (Mu et al., 2022), SigLIP (Zhai et al., 2023), and FLAIR (Xiao et al., 2025). When pretrained on CC3M, CC12M and YFCC15M, ITO achieves substantial improvements across a wide range of benchmarks, demonstrating stronger and more robust visual representations. As the pretraining scale increases, these gains remain stable. On Laion100M, ITO improves average zero-shot accuracy by 2.6% over CLIP. On the billion-scale DataComp-1B dataset, both ITO and ITO_sub2 achieve the strongest overall performance among all compared methods under the same backbone setting. Results with larger backbones and extended training are reported in the appendix Section C.

We further analyze the effect of textual diversity through sub-description sampling. On CC3M and CC12M, the ITO_sub2 configuration consistently improves performance over the default ITO, indicating that additional textual views can enhance contrastive supervision under moderate data regimes. Due to computational constraints, we do not apply sub-description sampling when pretraining on Laion100M. On DataComp-1B, we report results for both ITO and ITO_sub2. We observe that the performance difference between the two variants becomes marginal at this scale, suggesting that large-scale web data already provides sufficiently diverse textual supervision. Accordingly, we adopt the default ITO configuration for all large-scale experiments.

Overall, these results show that ITO achieves strong and stable zero-shot generalization across data scales. Combined with our analysis in Section 4.7, this suggests that while enriched alignment contributes most of the accuracy gains, training-time multimodal fusion plays a complementary role in improving representation robustness and generalization.

Table 1. Top-1 zero-shot classification accuracy on 26 public benchmarks following the EVA-CLIP (Sun et al., 2023) protocol. Benchmarks include ImageNet-1K (Deng et al., 2009), ImageNet-A (Hendrycks et al., 2021b), ImageNet-R (Hendrycks et al., 2021a), CIFAR-10/100 (Krizhevsky et al., 2009), Food-101 (Bossard et al., 2014), Pets (Parkhi et al., 2012), SUN397 (Xiao et al., 2010), FGVC Aircraft (Maji et al., 2013), EuroSAT (Helber et al., 2019), VOC2007 (Everingham et al., 2015), etc. The best results are highlighted in **bold**.

	ImageNet-1k	ImageNet-A	ImageNet-R	ImageNet-S	ImageNet-V2	ObjectNet	CIFAR-10	CIFAR-100	Flowers-102	Food-101	Pets	Stanford Cars	MNIST	Caltech	SUN397	FGVC Aircraft	Country-211	DTD	EuroSAT	FER2013	GTSRB	PCam	Rendered SST2	Resisc45	STL10	VOC2007	Avg
(a) *Results on CC3M (ViT-B/16, 30 epochs)*																											
CLIP	14.8	3.2	16.0	6.0	12.7	7.8	45.5	17.8	11.6	9.4	10.4	0.7	10.2	49.8	22.3	1.6	0.5	12.5	6.0	27.3	4.5	55.6	49.9	17.4	70.3	18.5	19.3
SLIP	18.3	5.1	19.6	8.1	15.5	10.5	47.0	19.0	10.9	13.0	10.4	1.2	10.1	56.6	31.2	1.6	0.7	12.6	6.4	18.1	2.8	55.9	50.1	17.5	88.1	27.2	21.4
SigLIP	16.6	3.6	19.6	7.6	14.6	9.8	51.3	16.8	10.6	10.1	8.0	1.0	14.0	46.2	21.1	0.9	0.6	16.4	5.6	16.4	11.0	43.2	50.1	24.4	66.6	16.6	19.3
FLAIR	19.3	4.6	19.4	8.5	16.6	11.3	63.2	29.6	13.5	12.8	9.9	1.0	8.2	61.6	30.6	0.9	0.7	12.5	4.7	26.8	5.2	57.2	50.1	27.6	83.1	25.2	23.2
ITO	23.3	5.6	29.0	16.2	19.9	11.8	65.0	26.1	17.1	13.7	14.3	1.7	17.9	62.9	32.4	1.1	0.7	12.7	13.8	21.4	9.3	48.4	50.1	25.9	85.6	21.9	**24.9**
ITO_sub2	23.1	4.7	28.1	16.2	19.8	12.2	57.7	26.9	13.6	13.6	13.7	1.7	10.1	66.1	31.5	1.0	0.8	11.1	14.9	26.9	6.8	59.6	50.0	27.6	88.1	21.4	**24.9**
(b) *Results on CC12M (ViT-B/16, 30 epochs)*																											
CLIP	36.7	8.5	45.6	24.5	31.5	22.4	70.4	38.1	32.5	45.6	59.7	21.0	9.6	72.0	42.6	2.2	4.7	17.6	5.7	29.6	12.9	54.3	50.0	36.4	88.0	24.2	34.1
SLIP	40.9	12.4	50.7	28.8	34.7	27.6	72.6	46.6	32.9	48.8	54.0	20.7	9.0	74.9	43.8	2.7	5.4	22.6	11.5	31.7	7.9	50.0	48.8	32.1	91.3	33.2	36.0
SigLIP	40.6	11.3	53.0	28.7	35.1	25.2	76.5	41.0	27.8	38.1	48.4	20.9	12.9	71.4	42.1	2.6	5.0	27.1	10.2	20.9	11.4	53.5	49.6	41.2	88.7	27.5	35.0
FLAIR	41.5	10.4	51.2	30.2	34.9	25.5	73.5	38.3	30.5	47.6	60.8	22.2	4.6	75.4	47.9	2.0	6.2	19.4	7.2	22.8	10.7	51.8	49.9	39.3	89.1	29.6	35.5
ITO	45.5	12.7	60.6	36.0	39.3	28.6	76.7	47.5	34.9	54.1	62.0	30.0	10.3	79.1	50.8	3.2	5.7	23.7	1.2	19.7	7.7	50.0	50.2	44.9	95.4	27.7	38.4
ITO_sub2	47.0	13.1	60.9	38.4	40.6	29.5	84.2	51.2	39.9	57.0	69.7	33.1	11.9	77.4	53.3	3.7	7.8	25.5	4.2	17.6	13.1	50.9	49.9	45.3	94.8	30.4	**40.4**
(c) *Results on YFCC15M (ViT-B/16, 30 epochs)*																											
CLIP	36.4	20.2	22.9	9.4	31.9	17.6	71.6	36.9	53.6	41.6	22.6	2.7	10.2	65.1	37.6	2.7	7.1	16.7	16.6	26.3	4.4	51.9	50.0	24.6	86.1	25.6	30.5
ITO	44.3	25.6	32.7	16.8	38.6	22.8	70.4	40.6	60.6	50.8	30.9	4.5	10.5	72.8	47.2	2.4	8.4	22.4	7.1	24.3	7.2	55.0	50.4	31.7	94.0	23.8	34.5
ITO_sub2	44.4	25.2	34.1	16.0	39.1	22.5	75.5	38.3	63.2	54	36.9	3.9	10.0	74.0	48.9	3.8	8.8	26.2	7.8	22.2	8.2	53.3	50.0	29.4	95.2	28.8	**35.4**
(d) *Results on Laion100M (ViT-B/16, 30 epochs)*																											
CLIP	59.0	21.8	69.2	44.1	51.4	43.7	91.0	69.8	54.8	79.4	82.7	76.6	63.6	81.5	61.7	11.1	13.5	45.4	3.1	36.4	38.2	51.0	54.6	56.0	95.5	34.9	53.5
SLIP	55.4	21.0	65.7	41.7	48.5	43.1	89.9	68.9	51.5	75.3	74.3	72.7	57.0	81.2	58.6	9.2	11.5	45.3	1.8	42.9	35.5	50.3	50.6	50.7	93.8	36.2	51.3
ITO	62.8	25.6	75.5	50.2	54.8	46.2	93.8	75.0	61.4	81.9	83.6	81.7	58.1	83.8	64.6	13.7	13.9	50.1	2.7	40.6	40.7	50.3	54.4	60.2	97.0	35.8	**56.1**
(e) *Results on DataComp-1B (ViT-B/16, 1 epoch)*																											
CLIP	63.1	24.1	67.9	47.3	54.7	50.0	92.1	74.6	63.7	83.1	84.0	76.9	55.1	82.1	62.8	14.2	13.9	42.1	3.1	25.0	38.8	50.8	49.8	58.1	95.3	35.4	54.2
ITO	65.9	25.0	72.9	53.3	57.2	51.9	94.9	78.3	70.5	83.9	86.6	83.5	57.3	83.4	64.9	18.1	14.7	46.0	3.9	24.4	35.5	53.5	51.7	60.2	96.4	37.8	56.6
ITO_sub2	65.7	26.9	74.0	53.5	57.0	52.2	95.1	78.5	67.0	84.5	85.8	82.3	57.0	82.0	64.7	16.3	14.9	47.8	3.2	29.5	42.1	58.4	51.4	57.8	96.7	37.4	**57.0**

4.3. Linear Image Classification

We further evaluate the quality of learned visual representations via linear probing. Following standard practice, we train a linear classifier on top of frozen visual features for 30 epochs using AdamW with a cosine learning-rate schedule. Top-1 accuracy is reported in Figure 2, Figure 3, and Table 2.

Across all pretraining datasets, ITO consistently outperforms CLIP and prior image–text contrastive baselines under linear evaluation, indicating improved linear separability of the learned visual representations. When pretrained on YFCC15M and Laion100M, ITO achieves clear gains of 2–8% in average Top-1 accuracy over CLIP, demonstrating that the representations learned with training-time fusion transfer effectively to downstream classification with minimal supervision.

On the billion-scale DataComp-1B dataset, both data scale and model capacity further enhance performance. With

Table 2. Linear image classification of ITO and its variants pretrained on YFCC15M, Laion100M and DataComp-1B. The best results are highlighted in **bold**. † indicates models trained for 10 epochs using ViT-B/16. * indicates models trained for 1 epochs using ViT-L/16.

Dataset	Method	IN-1k	Flowers	Cars	Pets	Food	Avg
15M	CLIP	51.82	85.17	19.60	53.61	69.18	55.88
	ITO	**60.52**	92.18	**28.37**	61.22	**76.50**	63.76
	ITO_sub2	60.40	**92.37**	27.73	**62.82**	76.22	**63.91**
100M	CLIP	67.27	86.65	87.17	82.88	85.35	81.86
	ITO	**68.70**	**90.21**	**88.16**	**84.49**	**86.22**	**83.56**
1B	CLIP	67.39	90.08	87.14	79.61	86.47	82.14
	ITO	69.87	**92.47**	**90.70**	81.88	87.75	82.53
	ITO_sub2	**70.76**	92.24	90.34	**83.16**	**88.51**	**83.00**
	CLIP†	74.99	94.67	91.64	87.90	91.89	87.62
	ITO†	**76.20**	**96.16**	**92.89**	88.09	**92.54**	**89.18**
	ITO_sub2†	75.83	94.96	92.23	**89.37**	92.19	88.92
	CLIP*	73.78	93.04	90.23	86.54	90.83	86.88
	ITO*	**75.97**	**95.80**	92.28	87.84	**92.27**	**88.83**
	ITO_sub2*	74.88	94.89	**92.29**	**88.93**	91.43	88.48

Table 3. Zero-shot image-text retrieval on validation splits for standard benchmarks (MSCOCO and Flickr30k). The best results are highlighted in **bold**.

Dataset	Method	MSCOCO				Flickr30k			
		I → T		T → I		I → T		T → I	
		R@1	R@5	R@1	R@5	R@1	R@5	R@1	R@5
3M	CLIP	12.36	30.98	8.14	22.68	23.57	50.69	16.98	37.65
	SigLIP	13.70	32.66	9.28	23.48	28.90	53.25	18.32	39.43
	FLAIR	17.86	38.90	12.59	30.38	35.40	62.13	25.74	49.86
	ITO	**21.56**	45.36	**14.56**	33.71	**42.6**	**71.2**	**29.45**	**53.89**
	ITO_sub2	21.08	**45.62**	14.01	**33.88**	42.11	69.43	28.26	53.08
12M	CLIP	34.17	61.20	23.04	47.58	62.23	86.29	45.74	73.02
	SigLIP	39.98	67.28	26.85	51.48	68.34	89.45	50.87	75.96
	FLAIR	36.20	63.16	24.62	48.79	62.92	88.56	47.36	74.77
	ITO	42.30	70.00	29.62	55.74	**72.49**	90.83	54.50	79.98
	ITO_sub2	**43.94**	**70.40**	**30.51**	**56.76**	72.29	**92.80**	**56.65**	**82.54**
15M	CLIP	26.38	50.86	15.06	34.82	47.14	74.46	30.77	56.82
	ITO	30.76	57.44	19.57	41.61	54.83	82.74	35.72	62.60
	ITO_sub2	**31.42**	**58.02**	**20.04**	**42.88**	**56.21**	**83.14**	**37.95**	**65.46**
100M	CLIP	49.12	74.66	31.92	57.32	75.94	93.59	60.04	84.08
	ITO	**52.08**	**76.04**	**34.26**	**59.57**	**79.59**	**95.66**	**63.00**	**86.21**
1B	CLIP	47.08	72.70	29.51	54.84	72.68	90.63	54.73	80.49
	ITO	49.26	**74.76**	31.30	56.63	**75.94**	**94.08**	**56.79**	82.17
	ITO_sub2	**49.50**	74.12	**31.89**	**57.26**	73.37	93.00	55.70	**82.33**
	CLIP†	57.70	80.86	37.76	63.58	82.25	96.65	66.57	87.71
	ITO†	**58.14**	**81.76**	**38.97**	**64.45**	**84.81**	**96.45**	**67.10**	**88.38**
	ITO_sub2†	55.88	79.90	38.33	64.03	81.95	95.36	65.88	87.67
	CLIP*	53.40	77.76	34.88	60.16	78.40	95.07	62.60	85.62
	ITO*	**56.58**	**80.46**	**38.12**	**63.72**	**83.14**	**96.35**	**66.33**	**87.69**
	ITO_sub2*	52.12	77.44	35.69	61.62	78.99	95.27	62.88	85.42

ViT-B/16 pretrained for 10 epochs, ITO reaches an average accuracy of 89.18%, exceeding CLIP by 1.56 points. Notably, the ViT-L/16 model, despite being trained for only one epoch, achieves 88.83%, highlighting the robustness and scalability of the proposed training strategy. We also report results with sub-description sampling on DataComp-1B. Consistent with zero-shot classification, the performance difference between ITO and ITO_sub2 becomes marginal at this scale, suggesting that large-scale pretraining already provides sufficiently rich textual supervision. Overall, these results confirm that ITO learns visual representations with strong linear separability and stable generalization across data scales.

4.4. Zero-shot Image–Text Retrieval

We evaluate zero-shot image–text retrieval to assess cross-modal alignment quality using MSCOCO (Lin et al., 2014) and Flickr30k (Plummer et al., 2015). Following standard practice, we report bidirectional retrieval performance, including image-to-text (I→T) and text-to-image (T→I) recall. To improve readability, we report Recall@1 and Recall@5 in the main paper, while the complete Recall@10 results are provided in the appendix Table 13. Only the pretrained vision and text encoders are used during evaluation.

As summarized in Table 3, ITO consistently outperforms CLIP, SLIP, and FLAIR across most pretraining datasets and retrieval directions, demonstrating stronger cross-modal alignment under the standard dual-encoder setting. On medium-scale datasets such as CC3M, CC12M, and YFCC15M, incorporating sub-description sampling (ITO_sub2) further improves retrieval performance, indicating that richer textual views can enhance alignment when data diversity is limited. At larger scales, the advantage of training-time fusion becomes more pronounced, while the effect of text augmentation diminishes. On the billion-scale DataComp-1B dataset, the baseline ITO achieves the highest overall recall for both ViT-B/16 (10 epochs) and ViT-L/16 (1 epoch), outperforming all compared baselines. In contrast, ITO_sub2 provides marginal or no improvement at this scale, suggesting that large-scale pretraining already supplies sufficient textual diversity for robust alignment.

Table 4. The performance of ITO on a broad range of multimodal tasks. The best results are **bold**.

Dataset	Method	VQAv2	GQA	T-VQA	SciQA-I	VisWiz	MMB-en	MMB-cn	MMVet	POPE-r	POPE-p	POPE-a	MMMU	MMStar
100M	CLIP	66.53	56.36	47.55	65.44	36.80	53.69	46.13	18.30	84.09	82.90	76.40	33.60	28.87
	ITO	**68.47**	**57.23**	**48.71**	**66.29**	**44.25**	**54.12**	**46.65**	**19.80**	**84.74**	**83.63**	**77.30**	**33.90**	**29.13**
1B	CLIP	70.42	57.93	50.24	65.00	**45.28**	48.45	55.67	18.40	83.63	82.71	78.63	**34.00**	29.33
	ITO	**73.19**	**59.99**	**50.89**	**66.24**	42.92	**50.52**	**58.85**	**21.90**	**85.46**	**84.23**	**80.46**	33.90	**31.13**

We additionally evaluate fine-grained image–text retrieval on the DOCCI benchmark (Onoe et al., 2024), which provides an average of seven sentence-level descriptions per image. Detailed results are reported in Appendix Table 14. Since retrieval tasks rely heavily on the precise geometric proximity of image and text embeddings, the consistent improvements of ITO over baselines (especially on fine-grained benchmarks like DOCCI) provide strong empirical evidence for the superior structural integrity of our learned embedding space. The fusion module ensures that semantically related pairs are pulled closer in a unified space, which is critical for ranking tasks.

4.5. Transfer to MLLM Benchmarks

Many multimodal large language models rely on a pre-trained vision encoder as a fixed perceptual backbone. To evaluate the transferability of learned visual representations, we follow the LLaVA-1.5 (Liu et al., 2024a) protocol and integrate Vicuna-7B (Chiang et al., 2023) with vision encoders pretrained using CLIP and ITO, all based on ViT-B/16. Unless otherwise specified, the vision encoder is frozen during multimodal fine-tuning, isolating the effect of visual pre-training.

We evaluate models pretrained on Laion100M and on the 10-epoch version of DataComp-1B across 13 Multimodal Large Language Model benchmarks, including VQAv2 (Goyal et al., 2017b), GQA (Ainslie et al., 2023), T-VQA (Singh et al., 2019), SciQA (Lu et al., 2022), VizWiz (Gurari et al., 2018), MMBench (Liu et al., 2024b), MMVet (Yu et al., 2024), POPE (Li et al., 2023), MMMU (Yue et al., 2024), and MMStar (Chen et al., 2024b).

As shown in Table 4, vision encoders pretrained with ITO-

Table 5. Ablation study on YFCC15M. We analyze the effect of Multimodal Multiple Alignment and training-time multimodal fusion by varying the fusion weight λ (left) and the number of Sentence Blocks (right). Results are zero-shot Top-1 accuracy (%) on ImageNet-1K using ViT-B/16. The baseline is standard CLIP.

Method	λ	Top-1
Baseline	-	36.4
ITO	0	43.7
ITO	2	**44.3**
ITO	4	44.0
ITO	6	43.2
ITO	8	43.6

Method	Blocks	Top-1
Baseline	-	36.4
ITO	1	43.9
ITO	2	**44.3**
ITO	3	43.7
ITO	4	43.5
ITO	5	44.0

consistently outperform their CLIP counterparts across all evaluated benchmarks. The improvements are particularly pronounced on reasoning-intensive datasets such as VQAv2, GQA, MMVet, and POPE, indicating that stronger visual representations benefit downstream multimodal reasoning even when the language model remains unchanged. Moreover, pretraining on the billion-scale DataComp-1B dataset leads to the highest overall performance, further highlighting the scalability of our approach.

Our results on complex reasoning tasks suggest that the modality-agnostic structure of ITO's embedding space significantly lowers the adaptation barrier for Large Language Models. This improved structural alignment reduces the burden on the projection layer during instruction tuning, allowing the MLLM to focus on higher-order reasoning rather than bridging low-level modality discrepancies.

4.6. Ablation Study

We conduct ablation experiments on YFCC15M using ViT-B/16 to analyze the contribution of each component in ITO. All results are reported as zero-shot Top-1 accuracy on ImageNet-1K, with detailed numbers provided in Table 5.

Synergy of Multimodal Multiple Alignment and Fusion. We first examine the interplay between multimodal multiple alignment and the fusion loss weight λ (Table 5, left). Compared to the standard CLIP baseline, introducing multiple alignment substantially boosts performance, confirming that constructing diverse image–text correspondences is effective for mining the discriminative potential of the data. Crucially, enabling training-time multimodal fusion ($\lambda > 0$) further enhances performance, with the best results achieved under moderate fusion strength. While the absolute accuracy gain from fusion might appear secondary to alignment, our analysis in Section 4.7 reveals its critical role as a structural regularizer. Overly large λ leads to degradation, reflecting the need to balance the dual-encoder's independence with cross-modal guidance.

Effect of Fusion Module Depth. We further vary the depth of the fusion module by changing the number of Sentence Blocks (Table 5, right). A shallow fusion design is sufficient to trigger the regularization effect, improving performance over the alignment-only setting. Increasing depth beyond two blocks yields diminishing returns, confirming that the fusion module acts primarily as a *training signal* to guide the gradient flow of the encoders, rather than requiring deep semantic reasoning itself. Overall, the ablations demonstrate a distinct division of labor: multiple alignment maximizes the information intake, while training-time fusion ensures the geometric integrity of the learned space.

4.7. Analysis

We analyze the role of training-time fusion beyond simple accuracy metrics, focusing on representation geometry and training dynamics. Additional visualizations are provided in Appendix Figure 5 and Figure 8.

Alignment vs. Integration. Although multimodal multiple alignment ($\lambda = 0$) drives strong downstream performance, representations learned under this regime remain partially organized by modality, suggesting the model relies on modality-specific shortcuts. In contrast, enabling training-time fusion ($\lambda > 0$) consistently eliminates this modality separation, yielding a unified semantic space where images and texts are interleaved. This confirms that the fusion objective successfully propagates gradient signals back to the individual encoders, forcing them to learn structurally integrated representations even though the fusion module is discarded at inference.

Fusion as a Stabilizer. We further examine training dynamics on YFCC15M to highlight the regularization effect of fusion. As shown in Appendix Figure 8, standard contrastive methods like CLIP and SLIP are prone to overfitting, exhibiting early saturation (peak accuracy at epoch 26) followed by performance degradation. This behavior has also been noted in prior studies of SLIP. While introducing multimodal multiple alignment ($\lambda = 0$) delays this overfitting (peak at epoch 28), it does not fundamentally solve the instability, as performance still tends to decline in later epochs. In sharp contrast, enabling training-time multimodal fusion ($\lambda = 2$) stabilizes the training dynamics, leading to consistent performance improvements throughout the full 30-epoch schedule without an early peak. This observation highlights that fusion serves as a critical **structural regularizer**, preventing the model from overfitting to noise in aggressive alignment settings and enabling scalable training.

5. Conclusion

In this work, we demonstrated that strong alignment in contrastive pretraining does not guarantee integrated representations, as modality gaps often persist. To address this,

we proposed **ITO**, which synergizes multimodal multiple alignment with a training-time fusion objective. Our analysis reveals that while alignment drives discriminative power, fusion acts as a critical **structural regularizer** that unifies the embedding space and stabilizes training dynamics. Crucially, by discarding the fusion module at inference, ITO achieves superior representation quality while preserving the efficiency of standard dual-encoder architectures, demonstrating that explicitly shaping representation structure is a key pathway to robust multimodal learning.

References

Ainslie, J., Lee-Thorp, J., de Jong, M., Zemlyanskiy, Y., Lebrón, F., and Sanghai, S. GQA: training generalized multi-query transformer models from multi-head checkpoints. In *EMNLP*, pp. 4895–4901, 2023.

Barbu, A., Mayo, D., Alverio, J., Luo, W., Wang, C., Gutfreund, D., Tenenbaum, J., and Katz, B. Objectnet: A large-scale bias-controlled dataset for pushing the limits of object recognition models. In *NeurIPS*, 2019.

Bossard, L., Guillaumin, M., and Van Gool, L. Food-101–mining discriminative components with random forests. In *ECCV*, 2014.

Changpinyo, S., Sharma, P., Ding, N., and Soricut, R. Conceptual 12m: Pushing web-scale image-text pre-training to recognize long-tail visual concepts. In *CVPR*, pp. 3558–3568, 2021.

Chen, L., Li, J., Dong, X., Zhang, P., He, C., Wang, J., Zhao, F., and Lin, D. Sharegpt4v: Improving large multi-modal models with better captions. In *ECCV*, pp. 370–387, 2024a.

Chen, L., Li, J., Dong, X., Zhang, P., Zang, Y., Chen, Z., Duan, H., Wang, J., Qiao, Y., Lin, D., and Zhao, F. Are we on the right way for evaluating large vision-language models? In *NeurIPS*, 2024b.

Chen, X., Xie, S., and He, K. An empirical study of training self-supervised vision transformers. In *ICCV*, pp. 9620–9629, 2021.

Cherti, M., Beaumont, R., Wightman, R., Wortsman, M., Ilharco, G., Gordon, C., Schuhmann, C., Schmidt, L., and Jitsev, J. Reproducible scaling laws for contrastive language-image learning. In *CVPR*, pp. 2818–2829, 2023.

Chiang, W.-L., Li, Z., Lin, Z., Sheng, Y., Wu, Z., Zhang, H., Zheng, L., Zhuang, S., Zhuang, Y., Gonzalez, J. E., Stoica, I., and Xing, E. P. Vicuna: An open-source chatbot impressing gpt-4 with 90%* chatgpt quality, March 2023. URL https://lmsys.org/blog/2023-03-30-vicuna/.

Cimpoi, M., Maji, S., Kokkinos, I., Mohamed, S., , and Vedaldi, A. Describing textures in the wild. In *CVPR*, 2014.

Dai, W., Li, J., Li, D., Tiong, A. M. H., Zhao, J., Wang, W., Li, B., Fung, P., and Hoi, S. C. H. Instructblip: Towards general-purpose vision-language models with instruction tuning. In *NeurIPS*, 2023.

Deng, J., Dong, W., Socher, R., Li, L.-J., Li, K., and Fei-Fei, L. Imagenet: A large-scale hierarchical image database. In *CVPR*, 2009.

Dou, Z., Kamath, A., Gan, Z., Zhang, P., Wang, J., Li, L., Liu, Z., Liu, C., LeCun, Y., Peng, N., Gao, J., and Wang, L. Coarse-to-fine vision-language pre-training with fusion in the backbone. In *NeurIPS*, 2022.

Dubey, A., Jauhri, A., Pandey, A., Kadian, A., Al-Dahle, A., Letman, A., Mathur, A., Schelten, A., Yang, A., Fan, A., Goyal, A., Hartshorn, A., Yang, A., Mitra, A., Sravankumar, A., Korenev, A., Hinsvark, A., Rao, A., Zhang, A., Rodriguez, A., Gregerson, A., Spataru, A., Rozière, B., Biron, B., Tang, B., Chern, B., Caucheteux, C., Nayak, C., Bi, C., Marra, C., McConnell, C., Keller, C., Touret, C., Wu, C., Wong, C., Ferrer, C. C., Nikolaidis, C., Allonsius, D., Song, D., Pintz, D., Livshits, D., Esiobu, D., Choudhary, D., Mahajan, D., Garcia-Olano, D., Perino, D., Hupkes, D., Lakomkin, E., AlBadawy, E., Lobanova, E., Dinan, E., Smith, E. M., Radenovic, F., Zhang, F., Synnaeve, G., Lee, G., Anderson, G. L., Nail, G., Mialon, G., Pang, G., Cucurell, G., Nguyen, H., Korevaar, H., Xu, H., Touvron, H., Zarov, I., Ibarra, I. A., Kloumann, I. M., Misra, I., Evtimov, I., Copet, J., Lee, J., Geffert, J., Vranes, J., Park, J., Mahadeokar, J., Shah, J., van der Linde, J., Billock, J., Hong, J., Lee, J., Fu, J., Chi, J., Huang, J., Liu, J., Wang, J., Yu, J., Bitton, J., Spisak, J., Park, J., Rocca, J., Johnstun, J., Saxe, J., Jia, J., Alwala, K. V., Upasani, K., Plawiak, K., Li, K., Heafield, K., Stone, K., and et al. The llama 3 herd of models. *CoRR*, abs/2407.21783, 2024.

Eslami, S. and de Melo, G. Mitigate the gap: Investigating approaches for improving cross-modal alignment in CLIP. In *ICLR*, 2025.

Everingham, M., Eslami, S. A., Van Gool, L., Williams, C. K., Winn, J., and Zisserman, A. The pascal visual object classes challenge: A retrospective. *IJCV*, 2015.

Fan, L., Krishnan, D., Isola, P., Katabi, D., and Tian, Y. Improving CLIP training with language rewrites. In *NeurIPS*, 2023.

Gadre, S. Y., Ilharco, G., Fang, A., Hayase, J., Smyrnis, G., Nguyen, T., Marten, R., Wortsman, M., Ghosh, D., Zhang, J., Orgad, E., Entezari, R., Daras, G., Pratt, S. M.,

Ramanujan, V., Bitton, Y., Marathe, K., Mussmann, S., Vencu, R., Cherti, M., Krishna, R., Koh, P. W., Saukh, O., Ratner, A. J., Song, S., Hajishirzi, H., Farhadi, A., Beaumont, R., Oh, S., Dimakis, A., Jitsev, J., Carmon, Y., Shankar, V., and Schmidt, L. Datacomp: In search of the next generation of multimodal datasets. In *NeurIPS 2023*, 2023.

Goel, S., Bansal, H., Bhatia, S., Rossi, R. A., Vinay, V., and Grover, A. Cyclip: Cyclic contrastive language-image pretraining. In *NeurIPS*, 2022.

Goyal, Y., Khot, T., Summers-Stay, D., Batra, D., and Parikh, D. Making the V in VQA matter: Elevating the role of image understanding in visual question answering. In *CVPR*, pp. 6325–6334, 2017a.

Goyal, Y., Khot, T., Summers-Stay, D., Batra, D., and Parikh, D. Making the V in VQA matter: Elevating the role of image understanding in visual question answering. In *CVPR*, pp. 6325–6334, 2017b.

Gurari, D., Li, Q., Stangl, A. J., Guo, A., Lin, C., Grauman, K., Luo, J., and Bigham, J. P. Vizwiz grand challenge: Answering visual questions from blind people. In *CVPR*, pp. 3608–3617, 2018.

Helber, P., Bischke, B., Dengel, A., and Borth, D. Eurosat: A novel dataset and deep learning benchmark for land use and land cover classification. *IEEE J. Sel. Top. Appl. Earth Obs. Remote Sens.*, 2019.

Hendrycks, D., Basart, S., Mu, N., Kadavath, S., Wang, F., Dorundo, E., Desai, R., Zhu, T., Parajuli, S., Guo, M., et al. The many faces of robustness: A critical analysis of out-of-distribution generalization. In *CVPR*, 2021a.

Hendrycks, D., Zhao, K., Basart, S., Steinhardt, J., and Song, D. Natural adversarial examples. In *CVPR*, 2021b.

Krizhevsky, A., Hinton, G., et al. Learning multiple layers of features from tiny images. 2009.

Lai, Z., Zhang, H., Zhang, B., Wu, W., Bai, H., Timofeev, A., Du, X., Gan, Z., Shan, J., Chuah, C., Yang, Y., and Cao, M. Veclip: Improving CLIP training via visual-enriched captions. In *ECCV*, volume 15100, pp. 111–127, 2024.

Li, Y., Du, Y., Zhou, K., Wang, J., Zhao, W. X., and Wen, J. Evaluating object hallucination in large vision-language models. In *EMNLP*, pp. 292–305, 2023.

Lin, T., Maire, M., Belongie, S. J., Hays, J., Perona, P., Ramanan, D., Dollár, P., and Zitnick, C. L. Microsoft COCO: common objects in context. In *ECCV*, volume 8693, pp. 740–755, 2014.

Liu, H., Li, C., Li, Y., and Lee, Y. J. Improved baselines with visual instruction tuning. In *CVPR*, pp. 26286–26296, 2024a.

Liu, Y., Duan, H., Zhang, Y., Li, B., Zhang, S., Zhao, W., Yuan, Y., Wang, J., He, C., Liu, Z., Chen, K., and Lin, D. Mmbench: Is your multi-modal model an all-around player? In *ECCV*, volume 15064, pp. 216–233, 2024b.

Lu, P., Mishra, S., Xia, T., Qiu, L., Chang, K., Zhu, S., Tafjord, O., Clark, P., and Kalyan, A. Learn to explain: Multimodal reasoning via thought chains for science question answering. In *NeurIPS*, 2022.

Maji, S., Rahtu, E., Kannala, J., Blaschko, M. B., and Vedaldi, A. Fine-grained visual classification of aircraft. *CoRR*, abs/1306.5151, 2013.

Mu, N., Kirillov, A., Wagner, D. A., and Xie, S. SLIP: self-supervision meets language-image pre-training. In *ECCV*, volume 13686, pp. 529–544, 2022.

Onoe, Y., Rane, S., Berger, Z., Bitton, Y., Cho, J., Garg, R., Ku, A., Parekh, Z., Pont-Tuset, J., Tanzer, G., Wang, S., and Baldridge, J. DOCCI: descriptions of connected and contrasting images. In *ECCV*, volume 15118, pp. 291–309, 2024.

Parkhi, O. M., Vedaldi, A., Zisserman, A., and Jawahar, C. V. Cats and dogs. In *CVPR*, 2012.

Plummer, B. A., Wang, L., Cervantes, C. M., Caicedo, J. C., Hockenmaier, J., and Lazebnik, S. Flickr30k entities: Collecting region-to-phrase correspondences for richer image-to-sentence models. In *ICCV*, pp. 2641–2649, 2015.

Radford, A., Kim, J. W., Hallacy, C., Ramesh, A., Goh, G., Agarwal, S., Sastry, G., Askell, A., Mishkin, P., Clark, J., Krueger, G., and Sutskever, I. Learning transferable visual models from natural language supervision. In *ICML*, volume 139, pp. 8748–8763, 2021.

Schuhmann, C., Vencu, R., Beaumont, R., Kaczmarczyk, R., Mullis, C., Katta, A., Coombes, T., Jitsev, J., and Komatsuzaki, A. LAION-400M: open dataset of clip-filtered 400 million image-text pairs. *CoRR*, abs/2111.02114, 2021.

Sharma, P., Ding, N., Goodman, S., and Soricut, R. Conceptual captions: A cleaned, hypernymed, image alt-text dataset for automatic image captioning. In *ACL*, pp. 2556–2565, 2018.

Singh, A., Natarajan, V., Shah, M., Jiang, Y., Chen, X., Batra, D., Parikh, D., and Rohrbach, M. Towards VQA models that can read. In *CVPR*, pp. 8317–8326, 2019.

Sun, Q., Fang, Y., Wu, L., Wang, X., and Cao, Y. EVA-CLIP: improved training techniques for CLIP at scale. *CoRR*, abs/2303.15389, 2023.

Torralba, A. and Efros, A. A. Unbiased look at dataset bias. In *CVPR*, pp. 1521–1528, 2011.

Veeling, B. S., Linmans, J., Winkens, J., Cohen, T., and Welling, M. Rotation equivariant cnns for digital pathology. In *MICCAI*, 2018.

Wang, H., Ge, S., Lipton, Z., and Xing, E. P. Learning robust global representations by penalizing local predictive power. *NeurIPS*, 2019.

Xiao, J., Hays, J., Ehinger, K. A., Oliva, A., and Torralba, A. Sun database: Large-scale scene recognition from abbey to zoo. In *CVPR*, 2010.

Xiao, R., Kim, S., Georgescu, M.-I., Akata, Z., and Alaniz, S. Flair: Vlm with fine-grained language-informed image representations. In *CVPR*, 2025.

Xu, H., Xie, S., Tan, X. E., Huang, P., Howes, R., Sharma, V., Li, S., Ghosh, G., Zettlemoyer, L., and Feichtenhofer, C. Demystifying CLIP data. In *ICLR*. OpenReview.net, 2024.

Yu, W., Yang, Z., Li, L., Wang, J., Lin, K., Liu, Z., Wang, X., and Wang, L. Mm-vet: Evaluating large multimodal models for integrated capabilities. In *ICML*, 2024.

Yue, X., Ni, Y., Zheng, T., Zhang, K., Liu, R., Zhang, G., Stevens, S., Jiang, D., Ren, W., Sun, Y., Wei, C., Yu, B., Yuan, R., Sun, R., Yin, M., Zheng, B., Yang, Z., Liu, Y., Huang, W., Sun, H., Su, Y., and Chen, W. MMMU: A massive multi-discipline multimodal understanding and reasoning benchmark for expert AGI. In *CVPR*, pp. 9556–9567, 2024.

Zhai, X., Mustafa, B., Kolesnikov, A., and Beyer, L. Sigmoid loss for language image pre-training. In *ICCV*, pp. 11941–11952, 2023.

Zhao, W., Huang, Z., Feng, J., and Wang, X. Superclip: Clip with simple classification supervision, 2025. URL https://arxiv.org/abs/2512.14480.

Zheng, K., Zhang, Y., Wu, W., Lu, F., Ma, S., Jin, X., Chen, W., and Shen, Y. Dreamlip: Language-image pre-training with long captions. In *ECCV*, volume 15076, pp. 73–90, 2024.

Table 6. The original and actual downloaded number of image-text pairs in pretraining datasets.

Dataset	CC3M (Sharma et al., 2018)	CC12M (Changpinyo et al., 2021)	YFCC15M (Torralba & Efros, 2011)	Laion100M (Schuhmann et al., 2021)	DataComp-1B (Gadre et al., 2023)
Origin	3.32M	12.42M	15.39M	361.02M	1.40B
Download	2.91M	10.97M	14.08M	107.75M	1.03B

Table 7. Common ITO hyperparameters on Datacomp-1B.

Config	Value
Optimizer	AdamW
Learning rate	5e-4
Weight decay	0.1
Optimizer momentum	β_1=0.9, β_2=0.98
Batch size	16384(ViT-B), 8192(ViT-L)
Warm-up iterations	500
λ	2
Scale	(0.5,1.0)
Gray_scale_prob	0.2
Color_jitter	[0.4, 0.4, 0.4, 0.1]
Color_jitter_prob	0.8

A. Datasets

We conduct pretraining experiments on several widely used image–text datasets spanning different scales. All web-scale datasets, including CC3M (Sharma et al., 2018), CC12M (Changpinyo et al., 2021), Laion100M (a 100M subset of LAION-400M (Schuhmann et al., 2021)), and DataComp-1B (Gadre et al., 2023), are downloaded following the official `img2dataset` pipeline[1] with default configurations. For YFCC15M, we use the filtered English subset released by (Radford et al., 2021), which can be obtained via the public downloader[2].

Due to network availability and filtering, the number of successfully retrieved image–text pairs may differ from the nominal dataset size. The exact number of samples used for each dataset is summarized in Table 6.

B. Implementation Details

Table 7 summarizes the common hyperparameter settings used for pretraining ITO on the billion-scale DataComp-1B dataset. Unless otherwise specified, these configurations are shared across all ITO variants and baselines to ensure fair comparison.

All models are trained using the OpenCLIP framework. We adopt AdamW as the optimizer with standard momentum parameters and apply cosine learning-rate decay with linear warmup. The fusion loss weight λ is set to its default value as determined in the ablation study, and the fusion module consists of two lightweight Transformer blocks. Image resolution, tokenizer settings, batch size, and training schedules follow the standard CLIP protocol.

For baselines, we strictly follow the officially recommended hyperparameter settings. When reproducing baseline results, we use the same dataset versions and training pipelines as those used for ITO.

C. Zero-shot Results on DataComp-1B

We provide additional zero-shot classification results on the billion-scale DataComp-1B dataset to analyze the effect of training duration and model scale. All evaluations follow the same protocol as in the main paper and use standard CLIP-style prompts.

Effect of Training Epochs. We first study the impact of training duration using ViT-B/16. In addition to the 1-epoch setting reported in the main paper, we further train models for 10 epochs to examine scaling behavior with respect to

[1] https://github.com/rom1504/img2dataset
[2] https://github.com/AdamRain/YFCC15M_downloader.git

Table 8. Top-1 zero-shot classification accuracy on 26 public benchmarks following the EVA-CLIP (Sun et al., 2023) protocol. Results are reported for models pretrained on DataComp-1B with ViT-B/16 and ViT-L/16 as vision encoders. The best results are highlighted in **bold**.

	ImageNet-1k	ImageNet-A	ImageNet-R	ImageNet-S	ImageNet-V2	ObjectNet	CIFAR-10	CIFAR-100	Flowers-102	Food-101	Pets	Stanford Cars	MNIST	Caltech	SUN397	FGVC Aircraft	Country-211	DTD	EuroSAT	FER2013	GTSRB	PCam	Rendered SST2	Resisc45	STL10	VOC2007	Avg
(a) *Results on DataComp-1B (ViT-B/16, 1 epoch)*																											
CLIP	63.1	24.1	67.9	47.3	54.7	50.0	92.1	74.6	63.7	83.1	84.0	76.9	55.1	82.1	62.8	14.2	13.9	42.1	3.1	25.0	38.8	50.8	49.8	58.1	95.3	35.4	54.2
ITO	65.9	25.0	72.9	53.3	57.2	51.9	94.9	78.3	70.5	83.9	86.6	83.5	57.3	83.4	64.9	18.1	14.7	46.0	3.9	24.4	35.5	53.5	51.7	60.2	96.4	37.8	56.6
ITO_sub2	65.7	26.9	74.0	53.5	57.0	52.2	95.1	78.5	67.0	84.5	85.8	82.3	57.0	82.0	64.7	16.3	14.9	47.8	3.2	29.5	42.1	58.4	51.4	57.8	96.7	37.4	**57.0**
(b) *Results on DataComp-1B (ViT-B/16, 10 epochs)*																											
CLIP	72.0	45.7	81.2	58.6	64.7	62.7	95.7	80.8	74.4	90.2	92.0	86.7	79.3	84.7	69.7	25.4	21.4	59.4	2.2	39.9	54.1	62.8	51.3	66.1	97.7	37.3	63.7
ITO	73.5	45.7	83.2	62.0	66.3	63.6	96.9	83.5	75.8	90.8	91.1	89.2	81.1	85.1	70.3	30.8	21.8	61.4	7.3	37.8	55.5	57.7	50.5	69.9	98.3	38.3	**64.9**
ITO_sub2	72.1	42.8	82.9	60.7	64.4	62.9	96.7	82.7	74.0	89.7	90.8	87.3	76.6	85.4	69.8	27.2	21.0	60.4	4.8	32.4	45.9	56.5	52.4	66.7	98.1	38.1	63.2
(c) *Results on DataComp-1B (ViT-L/16, 1 epoch)*																											
CLIP	69.5	39.8	78.0	56.5	61.1	60.1	96.1	80.9	71.5	88.5	88.1	83.2	70.1	83.2	68.9	16.2	19.0	51.1	2.4	33.6	52.1	59.8	51.8	63.1	97.5	37.2	60.7
ITO	72.2	44.5	82.9	62.0	64.3	64.1	97.6	83.8	72.0	89.8	90.8	87.2	74.8	84.6	70.7	27.4	20.3	56.0	2.2	31.4	49.0	50.4	53.7	67.9	98.6	38.9	**63.0**
ITO_sub2	70.7	38.8	80.4	59.4	62.8	60.3	97.0	82.4	73.4	87.9	90.7	86.8	66.7	83.4	69.6	21.5	19.1	53.9	3.4	33.7	47.3	52.8	52.0	67.2	98.2	38.3	61.5

Table 9. Top-1 zero-shot classification accuracy on 26 public benchmarks following the EVA-CLIP (Sun et al., 2023) protocol. Results are reported for models pretrained on CC3M-recap with both ViT-B/16 as vision encoders. The best results are highlighted in **bold**.

	ImageNet-1k	ImageNet-A	ImageNet-R	ImageNet-S	ImageNet-V2	ObjectNet	CIFAR-10	CIFAR-100	Flowers-102	Food-101	Pets	Stanford Cars	MNIST	Caltech	SUN397	FGVC Aircraft	Country-211	DTD	EuroSAT	FER2013	GTSRB	PCam	Rendered SST2	Resisc45	STL10	VOC2007	Avg
(a) CC3M Pre-training ViT-B																											
FLAIR	27.7	7.6	31.4	15.0	23.8	15.5	73.9	44.3	18.9	19.8	25.9	2.5	13.1	69.8	42.3	1.6	2.6	18.8	7.4	30.6	11.4	45.7	50.1	34.6	92.9	26.6	29.0
ITO_sub2	30.4	8.8	38.8	19.9	27.2	16.1	62.7	38.0	19.7	23.1	29.9	3.6	18.5	71.4	46.0	2.6	2.6	20.5	7.1	22.4	11.9	50.0	50.1	37.3	94.4	27.1	**30.0**
ITO_sub3	30.9	9.4	39.5	20.7	26.7	16.3	62.2	36.1	20.0	23.1	30.2	4.2	16.8	72.1	46.0	1.2	2.6	21.3	8.5	19.6	10.2	50.0	50.1	35.0	94.0	22.5	29.6

optimization. As shown in Table 8, extending training consistently improves zero-shot performance across most benchmarks. Compared with CLIP, ITO exhibits more stable gains as training progresses, indicating improved utilization of large-scale data.

Effect of Model Scale. We further evaluate a larger ViT-L/16 model trained for 1 epoch on DataComp-1B. Despite the shorter training schedule, the ViT-L/16 variant achieves competitive or superior performance compared with ViT-B/16 trained for longer durations. This suggests that ITO benefits from model scaling and that training-time fusion remains effective when increasing model capacity.

Overall, these results demonstrate that ITO scales favorably with both training epochs and model size on billion-scale image–text data, while preserving the standard dual-encoder inference architecture.

D. Additional Experiments on CC3M-recap

To further investigate the impact of text augmentation, we conduct supplementary experiments on the CC3M-recap dataset, a synthetic dataset provided by Dreamlip (Zheng et al., 2024). In CC3M-recap, each original image–text pair (I, T) is processed by Vision–Language Models (VLMs) using two prompts—"Describe the image in detail" and "Describe the image in short"—to generate a long and a short caption, respectively. Moreover, by employing three different VLMs (InstructBLIP (Dai et al., 2023), LLaVA-1.5 (Liu et al., 2024a), and ShareGPT4V (Chen et al., 2024a)), each original pair yields six additional synthetic textual descriptions. This setup allows us to examine whether richer textual supervision can further enhance the performance of the proposed multimodal fusion framework.

Experimental Setup. Following the same training configurations as in the main experiments, we compare FLAIR (Xiao et al., 2025) with our text-augmented variants ITO_sub2 and ITO_sub3 on the CC3M-recap dataset. The original CC3M-

Table 10. Linear image classification of ITO and its variants pretrained on CC3M-recap.

Dataset	Method	ImageNet-1k	Flowers-102	Stanford Cars	Pets	Food-101
CC3M-recap	FLAIR	45.65	**76.57**	25.05	**67.05**	59.38
	ITO_sub2	52.43	73.64	23.96	65.09	64.15
	ITO_sub3	**53.05**	74.30	**25.32**	65.55	**64.70**

Table 11. Zero-shot image-text retrieval on validation splits for standard benchmarks (MSCOCO and Flickr30k).

Dataset	Method	MSCOCO						Flickr30k					
		I → T			T → I			I → T			T → I		
		R@1	R@5	R@10	R@1	R@5	R@10	R@1	R@5	R@10	R@1	R@5	R@10
CC3M-recap	FLAIR	37.54	64.38	75.88	29.76	55.53	66.69	65.19	87.08	92.41	53.25	78.01	85.48
	ITO_sub2	**47.76**	73.76	82.64	31.59	58.54	**69.98**	74.56	93.89	96.75	57.32	82.23	88.38
	ITO_sub3	47.40	**74.94**	**83.86**	**32.38**	**58.74**	69.77	**74.95**	**94.38**	**96.75**	**59.13**	**83.41**	**89.80**

Table 12. Zero-shot image-text retrieval on validation splits for fine-grained retrieval benchmarks (DOCCI).

Dataset	Method	DOCCI					
		I → T			T → I		
		R@1	R@5	R@10	R@1	R@5	R@10
CC3M-recap	FLAIR	20.16	43.56	54.66	10.65	24.23	31.60
	ITO_sub2	**27.82**	**54.14**	**65.90**	**10.70**	23.69	30.84
	ITO_sub3	27.54	53.68	65.30	10.68	**24.04**	**31.27**

recap dataset contains approximately 2.8 million image–text pairs, while we use about 1.7 million successfully downloaded samples in our experiments. For ITO_sub2 and ITO_sub3, we randomly sample two or three sub-descriptions from the long captions to construct multiple text views, respectively. All models are trained for 30 epochs using ViT-B/16 as the vision encoder. We evaluate them on the same downstream tasks as in the main paper, including 26 zero-shot classification datasets, linear probing for image classification, and image–text retrieval benchmarks.

Results. The results are summarized in Tables 9 to 12. Across all downstream tasks, incorporating richer textual supervision from CC3M-recap leads to consistent improvements over FLAIR (Xiao et al., 2025).

In the 26-dataset zero-shot classification benchmark (Table 9), both ITO_sub2 and ITO_sub3 outperform FLAIR by a clear margin, achieving average Top-1 accuracies of 30.0% and 29.6%, respectively. This demonstrates that our contrastive–fusion framework benefits from more diverse textual views even when trained on synthetic captions.

For linear probing (Table 10), ITO_sub2 and ITO_sub3 again show notable gains on ImageNet-1K and several fine-grained datasets, with ITO_sub3 achieving the best overall results (e.g., +7.4 points over FLAIR on ImageNet-1K). These findings indicate that long-caption sampling not only enhances zero-shot transfer but also improves the linear separability of learned visual features.

In zero-shot image–text retrieval (Table 11 and Table 12), our models consistently surpass FLAIR on both coarse-grained (MSCOCO, Flickr30k) and fine-grained (DOCCI) benchmarks. For instance, ITO_sub3 improves Recall@1 on MSCOCO I → T from 37.54% to 47.40%, and on Flickr30k from $65.19\%$to 74.95%. Similar gains are observed on DOCCI, confirming that text augmentation yields more robust and fine-grained alignment between images and captions.

Overall, these results validate the effectiveness of our text sampling strategy under the VLM-recaptioned setting. Richer and more diverse textual descriptions help our method capture finer semantic correspondences, while maintaining strong generalization across classification and retrieval tasks.

Discussion. These findings suggest that when captions are linguistically rich, sub-description sampling further enhances cross-modal learning by emphasizing diverse semantic aspects of the same image. Compared with the models pretrained on the original CC3M dataset, those trained on CC3M-recap achieve consistently higher performance across classification and retrieval benchmarks, confirming that richer textual supervision facilitates more effective image–text alignment. However,

Table 13. Zero-shot image-text retrieval on validation splits for standard benchmarks (MSCOCO and Flickr30k). The best results are highlighted in **bold**. † indicates models trained for 10 epochs using ViT-B/16. * indicates models trained for 1 epochs using ViT-L/16.

Dataset	Method	MSCOCO						Flickr30k					
		I → T			T → I			I → T			T → I		
		R@1	R@5	R@10	R@1	R@5	R@10	R@1	R@5	R@10	R@1	R@5	R@10
3M	CLIP	12.36	30.98	41.76	8.14	22.68	31.98	23.57	50.69	62.03	16.98	37.65	48.68
	SigLIP	13.70	32.66	43.16	9.28	23.48	32.60	28.90	53.25	65.09	18.32	39.43	49.45
	FLAIR	17.86	38.90	51.18	12.59	30.38	40.94	35.40	62.13	74.46	25.74	49.86	60.81
	ITO	**21.56**	45.36	57.22	**14.56**	33.71	44.90	**42.6**	**71.2**	**80.87**	**29.45**	**53.89**	**64.36**
	ITO_sub2	21.08	**45.62**	**57.42**	14.01	**33.88**	**45.06**	42.11	69.43	78.11	28.26	53.08	64.16
12M	CLIP	34.17	61.20	72.52	23.04	47.58	59.39	62.23	86.29	92.11	45.74	73.02	82.23
	SigLIP	39.98	67.28	77.82	26.85	51.48	63.20	68.34	89.45	93.29	50.87	75.96	84.18
	FLAIR	36.20	63.16	74.38	24.62	48.79	60.57	62.92	88.56	93.20	47.36	74.77	83.21
	ITO	42.30	70.00	79.46	29.62	55.74	67.09	**72.49**	90.83	95.07	54.50	79.98	86.86
	ITO_sub2	**43.94**	**70.40**	**80.26**	**30.51**	**56.76**	**68.29**	72.29	**92.80**	**96.35**	**56.65**	**82.54**	**88.58**
15M	CLIP	26.38	50.86	62.86	15.06	34.82	46.43	47.14	74.46	83.23	30.77	56.82	67.14
	ITO	30.76	57.44	68.82	19.57	41.61	53.03	54.83	82.74	88.56	35.72	62.60	73.06
	ITO_sub2	**31.42**	**58.02**	**69.06**	**20.04**	**42.88**	**54.61**	**56.21**	**83.14**	**90.43**	**37.95**	**65.46**	**75.50**
100M	CLIP	49.12	74.66	83.76	31.92	57.32	68.40	75.94	93.59	96.75	60.04	84.08	89.90
	ITO	**52.08**	**76.04**	**84.24**	**34.26**	**59.57**	**70.07**	**79.59**	**95.66**	**98.42**	**63.00**	**86.21**	**91.42**
1B	CLIP	47.08	72.70	82.64	29.51	54.84	66.05	72.68	90.63	94.48	54.73	80.49	87.53
	ITO	49.26	**74.76**	**83.62**	31.30	56.63	68.22	**75.94**	**94.08**	**97.14**	**56.79**	82.17	88.56
	ITO_sub2	**49.50**	74.12	83.06	**31.89**	**57.26**	**68.36**	73.37	93.00	96.15	55.70	**82.33**	**89.33**
	CLIP†	57.70	80.86	87.72	37.76	63.58	73.50	82.25	96.65	98.52	66.57	87.71	92.60
	ITO†	**58.14**	**81.76**	**88.88**	**38.97**	**64.45**	**74.63**	**84.81**	**96.45**	**98.52**	**67.10**	**88.38**	**93.18**
	ITO_sub2†	55.88	79.90	87.84	38.33	64.03	74.03	81.95	95.36	98.03	65.88	87.67	92.49
	CLIP*	53.40	77.76	86.62	34.88	60.16	71.04	78.40	95.07	97.63	62.60	85.62	91.26
	ITO*	**56.58**	**80.46**	**88.12**	**38.12**	**63.72**	**73.62**	**83.14**	**96.35**	**98.62**	**66.33**	**87.69**	**92.96**
	ITO_sub2*	52.12	77.44	85.96	35.69	61.62	71.86	78.99	95.27	98.03	62.88	85.42	91.20

as shown in the main paper (Sec. 4), this advantage becomes less pronounced on large-scale datasets such as DataComp-1B, where captions are typically short and less informative.

E. DOCCI and Full Zero-shot Retrieval Results

We provide additional zero-shot image–text retrieval results to complement the main paper. This section reports the complete Recall@1/5/10 metrics on MSCOCO and Flickr30k, as well as fine-grained retrieval performance on DOCCI.

Complete Retrieval Results on MSCOCO and Flickr30k. Table 13 report full bidirectional retrieval results (Image→Text and Text→Image) on the validation splits of MSCOCO and Flickr30k. These results extend the main paper, where only Recall@1 and Recall@5 are shown for clarity. The trends are consistent with those reported in the main text: ITO achieves strong and stable improvements over CLIP, SLIP, and FLAIR across datasets and retrieval directions, and the relative ordering of methods remains unchanged when considering Recall@10.

Fine-grained Retrieval on DOCCI. We further evaluate zero-shot retrieval on the DOCCI dataset, which provides an average of seven sentence-level descriptions per image and emphasizes fine-grained cross-modal matching. As shown in Table 14, ITO remains competitive across all recall metrics, demonstrating that representations learned via training-time fusion generalize well to detailed and compositional image–text retrieval scenarios. These results are consistent with the conclusions drawn from COCO and Flickr30k, and further validate the robustness of ITO under diverse retrieval settings.

Table 14. Zero-shot image-text retrieval on validation splits for fine-grained retrieval benchmarks (DOCCI). The best results are highlighted in **bold**. † indicates models trained for 10 epochs using ViT-B/16. * indicates models trained for 1 epochs using ViT-L/16.

Dataset	Method	DOCCI					
		I → T			T → I		
		R@1	R@5	R@10	R@1	R@5	R@10
3M	CLIP	4.10	12.56	18.72	2.13	6.71	10.07
	SigLIP	4.98	14.38	20.88	2.28	6.91	10.32
	FLAIR	7.12	19.12	28.00	3.23	9.70	14.13
	ITO	8.24	22.00	**31.64**	3.48	**9.97**	14.39
	ITO_sub2	**9.18**	**22.74**	31.20	**3.49**	9.96	**14.41**
12M	CLIP	20.14	43.40	53.54	7.67	17.96	24.03
	SigLIP	25.00	49.66	61.72	9.38	20.59	26.94
	FLAIR	24.24	48.50	59.12	9.36	21.20	28.11
	ITO	26.62	51.00	61.88	9.39	20.51	26.92
	ITO_sub2	**28.26**	**53.92**	**64.46**	**10.86**	**23.60**	**30.44**
15M	CLIP	15.94	35.26	45.70	5.45	13.54	18.81
	ITO	19.06	40.28	51.90	6.82	16.45	22.45
	ITO_sub2	**19.82**	**43.06**	**53.70**	**6.86**	**17.52**	**23.60**
100M	CLIP	39.28	65.30	74.68	13.04	25.45	31.81
	ITO	**41.54**	**67.48**	**76.52**	**13.68**	**26.48**	**32.80**
1B	CLIP	43.02	69.48	77.88	13.01	25.71	32.28
	ITO	43.24	69.98	79.26	13.75	26.78	33.27
	ITO_sub2	**44.08**	**70.86**	**79.56**	**14.47**	**28.31**	**35.01**
	CLIP†	52.58	76.98	84.78	16.66	30.49	37.09
	ITO†	**52.78**	**78.20**	**85.72**	17.30	31.60	38.30
	ITO_sub2†	50.78	76.18	83.78	**17.79**	**32.73**	**39.90**
	CLIP*	48.98	75.26	83.12	15.59	29.16	35.49
	ITO*	**50.94**	**76.56**	**84.36**	**16.77**	30.75	37.60
	ITO_sub2*	48.34	75.02	82.68	16.67	**30.95**	**38.01**

F. UMAP Visualization

F.1. CLIP vs. FLAIR vs. ITO: Modality Separation vs. Integration

We first compare the representation structures learned by CLIP, FLAIR, and ITO using UMAP visualization under identical settings. All models are trained on the CC3M dataset. For visualization, we randomly sample 8,192 image–text pairs from CC12M and project their embeddings into two dimensions using UMAP. Blue points represent image embeddings, and red points represent text embeddings.

As shown in Figure 4a, CLIP exhibits a clear separation between image and text embeddings, forming two modality-specific clusters with a distinct boundary. This observation is consistent with prior findings that instance-level contrastive alignment alone does not eliminate modality-induced organization in the embedding space.

Figure 4b presents the visualization for FLAIR. Compared with CLIP, FLAIR produces more compact text embeddings that are partially surrounded by image embeddings. This behavior is likely attributed to its text-conditioned pooling mechanism, which introduces localized fusion effects during training. However, the overall structure remains asymmetric, with text embeddings forming a concentrated region and images distributed more broadly, indicating that modality separation is alleviated but not fully resolved.

In contrast, Figure 6c shows the visualization for ITO. Image and text embeddings are more closely interwoven, forming a star-shaped distribution in which both modalities are mixed within shared neighborhoods. Notably, this visualization is obtained using only the standalone dual-encoder at inference time, without any fusion module. This suggests that the reduced modality separation is not an artifact of architectural unification, but rather reflects a change in the representation structure learned during training.

(a) CLIP *(b)* FLAIR *(c)* **ITO**

Figure 4. **UMAP visualization.** All models are trained on the CC3M dataset. For visualization, 8,192 image-text pairs are randomly sampled from CC12M. Blue points represent images, and red points represent texts. (a): CLIP exhibits a clear separation between modalities, with a distinct boundary between image and text embeddings. (b): FLAIR shows more compact text embeddings surrounded by image embeddings, likely due to its text-conditioned fusion mechanism. (c): Notably, ITOdemonstrates a star-shaped distribution, where image and text embeddings are more closely clustered together, effectively dissolving the boundary between modalities.

Taken together, these comparisons indicate that while alignment-focused methods such as CLIP and FLAIR improve cross-modal correspondence to varying degrees, training-time multimodal fusion in ITO leads to a qualitatively different organization of the embedding space, in which representations are less structured by modality and more tightly integrated.

F.2. Effect of Training-Time Fusion ($\lambda = 0$ vs. $\lambda > 0$)

(a) ITO ($\lambda = 0$) *(b)* ITO ($\lambda = 2$) *(c)* ITO_sub2

Figure 5. **UMAP visualization.** All models are trained on the CC3M dataset. For visualization, 8,192 image-text pairs are randomly sampled from CC12M. Blue points represent images, and red points represent texts.

To disentangle the effect of Multimodal Multiple Alignment from that of training-time multimodal fusion, we visualize the representation structures learned with different fusion weights. All models are trained on CC3M, and 8,192 image–text pairs are randomly sampled from CC12M for UMAP visualization. Inference is performed using the standalone dual-encoder in all cases.

Figure 5a shows the visualization for ITO with $\lambda = 0$, where only Multimodal Multiple Alignment is applied. Compared with CLIP, the separation between image and text embeddings is reduced, indicating improved instance-level alignment. However, the embedding space remains partially organized by modality, and a visible boundary between image and text representations persists.

Figure 5b presents the full ITO model with $\lambda = 2$. With training-time multimodal fusion enabled, image and text embeddings become more interwoven, and the modality-induced boundary is substantially weakened. This suggests that fusion loss introduces structured cross-modal interaction during training that reshapes the organization of the embedding space beyond what alignment alone can achieve.

Figure 5c further shows ITO_sub2, which incorporates both training-time fusion and sub-description sampling. The resulting embedding space exhibits the strongest degree of cross-modal mixing, with image and text representations densely

interleaved within shared neighborhoods. This indicates that while Multiple Alignment enriches supervision, fusion is essential for inducing deeper integration, and textual diversity further amplifies this effect under moderate data regimes.

These comparisons highlight a clear distinction between alignment and integration: Multiple Alignment improves correspondence between paired samples, whereas training-time multimodal fusion plays a crucial role in reducing modality-induced separation and shaping a more integrated representation structure.

F.3. CC3M-recap: FLAIR vs. ITO_sub2 vs. ITO_sub3

(a) FLAIR *(b)* ITO_sub2 *(c)* ITO_sub3

Figure 6. **UMAP visualization.** All models are trained on the CC3M-recap dataset. For visualization, 8,192 image-text pairs are randomly sampled from CC12M. Blue points represent images, and red points represent texts.

We conduct additional visualization analyses to further examine the behavior of our model across different fusion strategies and caption granularities. We first compare FLAIR (Xiao et al., 2025), ITO_sub2, and ITO_sub3 trained on the CC3M-recap dataset. As shown in Figure 6, FLAIR remains partially organized by modality on CC3M-recap, exhibiting limited cross-modal mixing, in contrast to its slightly more compact structure observed on the original CC3M dataset. This difference may be attributed to the fact that all subclauses in CC3M-recap originate from the same source caption, reducing the diversity of textual supervision.

In contrast, both ITO_sub2 and ITO_sub3 produce embedding spaces where image and text representations are more tightly interleaved. Rather than being separated by modality, representations are organized according to semantic similarity, indicating that ITO encourages deeper cross-modal integration beyond instance-level alignment.

F.4. DataComp-1B: CLIP vs. ITO

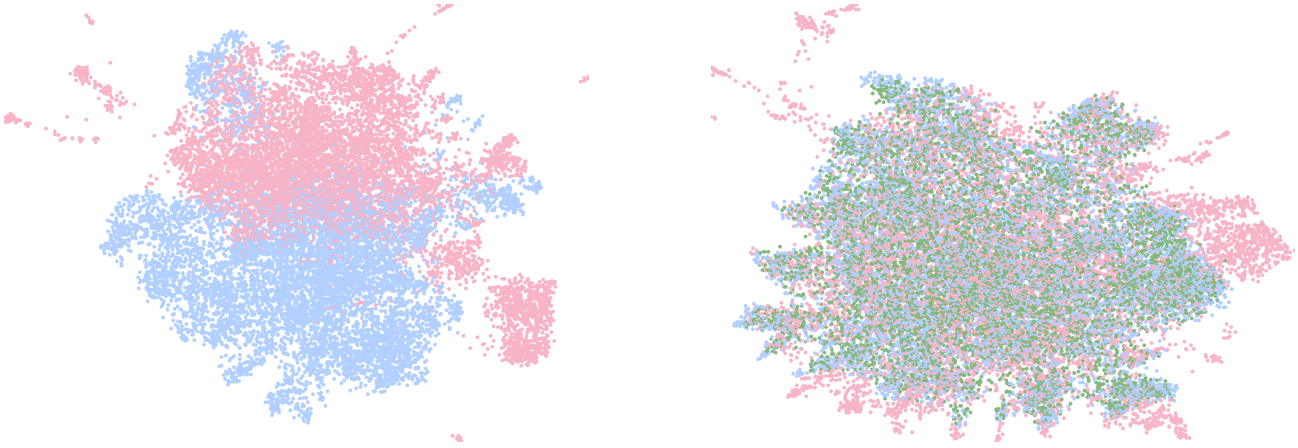

(a) CLIP *(b)* ITO

Figure 7. **UMAP visualization for DataComp-1B.** All models are trained on the DataComp-1B dataset for 10 epochs. For visualization, 8,192 image-text pairs are randomly sampled from CC12M. Blue points represent images, red points represent texts, and green points denote unified multimodal tokens. .

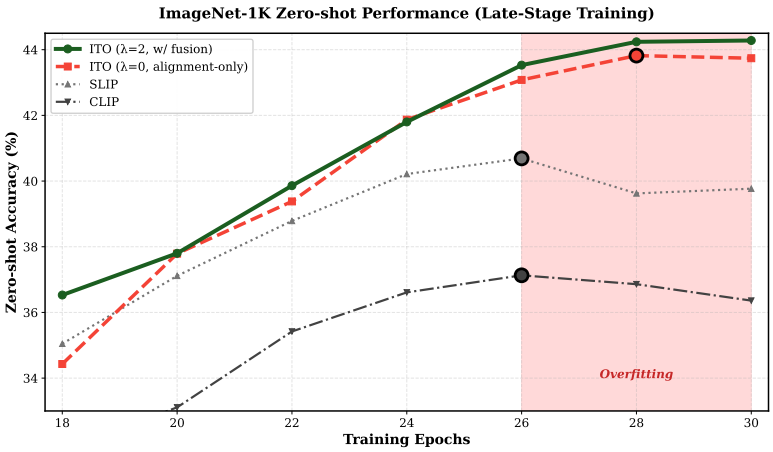

Figure 8. **Training dynamics and overfitting behavior on YFCC15M.** Zero-shot ImageNet-1K accuracy as a function of training epochs for CLIP, SLIP, and ITO variants using ViT-B/16. Both CLIP and SLIP exhibit late-stage performance degradation, indicating overfitting on moderately sized datasets. Introducing Multimodal Multiple Alignment alone (λ=0) improves overall accuracy but does not fully prevent overfitting. In contrast, enabling training-time multimodal fusion (λ=2) stabilizes training and maintains consistent zero-shot performance in later epochs, demonstrating the regularizing effect of fusion-based cross-modal interaction.

To investigate scalability, we further visualize models pretrained on the billion-scale DataComp-1B dataset. Specifically, we compare CLIP (Radford et al., 2021) and ITO using ViT-B/16, with both models pretrained for 10 epochs. For visualization, 8,192 image–text pairs are randomly sampled from CC12M to ensure stable and consistent comparison across different pretraining scales. Blue points represent image embeddings, red points denote text embeddings, and green points correspond to unified multimodal tokens.

As shown in Figure 7, CLIP exhibits a clear modality-induced separation, with image and text embeddings forming two distinct clusters. In contrast, ITO produces more intertwined and semantically organized distributions, where representations are less structured by modality and more by shared content. This observation indicates that training-time multimodal fusion continues to shape representation structure effectively, even under billion-scale pretraining.

G. Training Dynamics and Overfitting Analysis

To better understand the role of training-time multimodal fusion in image–text contrastive pretraining, we analyze the training dynamics of different methods by tracking zero-shot ImageNet-1K accuracy throughout training. All models are trained on YFCC15M using ViT-B/16, and evaluated under the standard CLIP zero-shot protocol.

Figure 8 reports the evolution of zero-shot accuracy for CLIP, SLIP, and our proposed ITO variants. Both CLIP and SLIP exhibit a clear late-stage performance degradation: after reaching peak accuracy, their zero-shot performance declines as training proceeds, indicating overfitting despite continued optimization. This behavior is consistent with prior observations in image–text contrastive learning on moderately sized datasets.

Introducing Multimodal Multiple Alignment alone (λ=0) substantially improves overall accuracy compared with CLIP and SLIP. However, this alignment-only variant still suffers from noticeable late-stage overfitting, as reflected by a similar peak-and-decline pattern in the training curve. This suggests that enriching instance-level contrastive supervision, while beneficial, is insufficient to fully stabilize training.

In contrast, enabling training-time multimodal fusion (λ=2) fundamentally changes the training dynamics. ITO exhibits consistently stable zero-shot performance in the later stages of training, without observable degradation. This indicates that the fusion objective provides an additional regularizing effect, guiding the encoders toward representations that generalize better and remain robust as training progresses.

Taken together, these results show that training-time multimodal fusion plays a critical role beyond multiple alignment alone. While multiple alignment strengthens correspondence between image–text pairs, fusion-based cross-modal interaction is essential for mitigating overfitting and stabilizing contrastive pretraining. Importantly, these benefits are achieved without introducing any additional inference-time cost, as the fusion module is discarded during deployment.

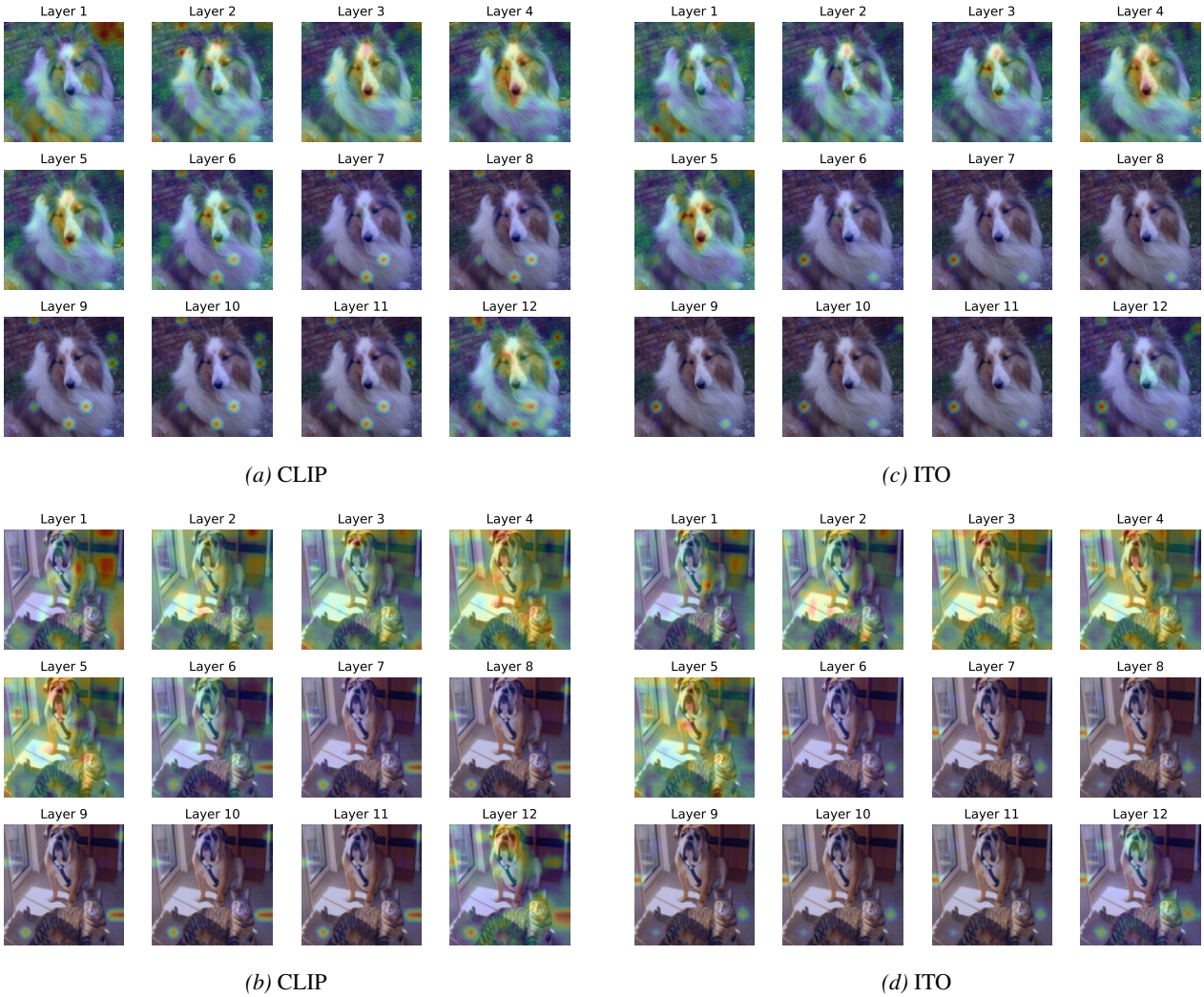

(a) CLIP *(c)* ITO

(b) CLIP *(d)* ITO

Figure 9. **Layer-wise attention visualization of CLIP and ITO on DataComp-1B.** Each image corresponds to a different transformer layer, with the layer index indicated above each visualization. ITO shows progressively more focused and semantically consistent attention distributions than CLIP. Note that all visualizations are derived from held-out samples rather than those seen during pretraining.

H. Layer-wise attention visualization

We visualize the attention maps across all 12 layers of the vision encoders from CLIP (Radford et al., 2021) and our ITO (trained for 10 epochs on DataComp-1B) to analyze their visual reasoning behaviors. As shown in Figure 9, ITO exhibits more concentrated and semantically coherent attention distributions across layers. From shallow to deep layers, the attention in ITO progressively evolves from dispersed low-level responses to high-level representations that focus on the semantic subject of the scene, while effectively suppressing background noise. This indicates that ITO forms a clearer hierarchical structure for semantic information aggregation and achieves stronger alignment between visual features and semantic content. In contrast, CLIP shows less stable attention evolution, with certain layers focusing on irrelevant background regions and exhibiting weaker inter-layer consistency. Overall, the representations learned by ITO are more structured and interpretable, demonstrating enhanced semantic consistency and better generalization capability.

I. Inference Efficiency.

ITO introduces a multimodal fusion module *only during training*. At inference time, the fusion module is entirely removed, and ITO reduces to a standard dual-encoder architecture identical to CLIP. As a result, ITO has the same number of parameters, computational cost, and inference latency as CLIP, and can be used as a drop-in replacement for existing

image–text contrastive encoders.

J. Training Overhead Analysis

To clarify the additional computational cost introduced by different training objectives, we analyze the relative training overhead of SigLIP, SLIP, and ITO with respect to the CLIP baseline. All comparisons are conducted under the same backbone, dataset (CC3M), batch size, and optimization settings, and are reported relative to CLIP.

In terms of training time, SigLIP incurs no additional overhead compared to CLIP. Both SLIP and ITO require approximately 1.4× the training time of CLIP, reflecting the additional objectives applied during optimization. Importantly, ITO does not introduce higher training-time cost than SLIP. Regarding GPU memory consumption, SigLIP requires a modest increase over CLIP (approximately 1.07×). SLIP exhibits a larger memory footprint (approximately 1.27×), while ITO remains more memory-efficient than SLIP, requiring approximately 1.15× the peak memory of CLIP. The additional memory usage in ITO is primarily due to the lightweight fusion module used during training.